PLOS | ONE

RESEARCH ARTICLE

Systemic siRNA Nanoparticle-Based Drugs Combined with Radiofrequency Ablation for Cancer Therapy

Muneeb Ahmed[1]*, Gaurav Kumar[1], Gemma Navarro[2], Yuanguo Wang[1], Svetlana Gourevitch[3], Marwan H. Moussa[1], Nir Rozenblum[3], Tatyana Levchenko[2], Eithan Galun[3], Vladimir P. Torchilin[2], S. Nahum Goldberg[1,4]

1 Laboratory for Minimally Invasive Tumor Therapies, Department of Radiology, Beth Israel Deaconess Medical Center/Harvard Medical School, 1 Deaconess Rd.–WCC-308B, Boston, Massachusetts, 02215, United States of America, **2** Department of Pharmaceutical Sciences and Center for Pharmaceutical Biotechnology and Nanomedicine, Northeastern University, 140 The Fenway, Boston, Massachusetts, 02115, United States of America, **3** The Goldyne Savad Institute of Gene Therapy, Hadassah Hebrew University Medical Center, Kiryat Hadassah POB 12000, Jerusalem, 91120, Israel, **4** Division of Image-guided Therapy and Interventional Oncology, Department of Radiology, Hadassah Hebrew University Medical Center, Kiryat Hadassah POB 12000, Jerusalem, 91120, Israel

* mahmed@bidmc.harvard.edu

Citation: Ahmed M, Kumar G, Navarro G, Wang Y, Gourevitch S, Moussa MH, et al. (2015) Systemic siRNA Nanoparticle-Based Drugs Combined with Radiofrequency Ablation for Cancer Therapy. PLoS ONE 10(7): e0128910. doi:10.1371/journal.pone.0128910

Editor: Yi-Hsiang Huang, National Yang-Ming University, TAIWAN

Received: March 19, 2015

Accepted: May 1, 2015

Published: July 8, 2015

Data Availability Statement: All relevant data are within the manuscript.

Funding: This work was supported by grants from the National Cancer Institute (CCNE 1U54CA151881-01 VPT, SNG, MA, TL), Radiological Society of North America Research and Education Foundation (RSD1215, MA), Harvard Medical Faculty Physicians Faculty Radiology Foundation (MA), Deutsche Forschungsgemeinschaft (SF8841, EG), the Israeli Center of Excellence I-CORE (EG), and the Israel Science Foundation (EG, SNG). The funders had no

Abstract

Purpose

Radiofrequency thermal ablation (RFA) of hepatic and renal tumors can be accompanied by non-desired tumorigenesis in residual, untreated tumor. Here, we studied the use of micelle-encapsulated siRNA to suppress IL-6-mediated local and systemic secondary effects of RFA.

Methods

We compared standardized hepatic or renal RFA (laparotomy, 1 cm active tip at 70±2°C for 5 min) and sham procedures without and with administration of 150nm micelle-like nanoparticle (MNP) anti-IL6 siRNA (DOPE-PEI conjugates, single IP dose 15 min post-RFA, C57Bl mouse:3.5 ug/100ml, Fisher 344 rat: 20ug/200ul), RFA/scrambled siRNA, and RFA/empty MNPs. Outcome measures included: local periablational cellular infiltration (α-SMA+ stellate cells), regional hepatocyte proliferation, serum/tissue IL-6 and VEGF levels at 6-72hr, and distant tumor growth, tumor proliferation (Ki-67) and microvascular density (MVD, CD34) in subcutaneous R3230 and MATBIII breast adenocarcinoma models at 7 days.

Results

For liver RFA, adjuvant MNP anti-IL6 siRNA reduced RFA-induced increases in tissue IL-6 levels, α-SMA+ stellate cell infiltration, and regional hepatocyte proliferation to baseline ($p<0.04$, all comparisons). Moreover, adjuvant MNP anti-IL6- siRNA suppressed increased distant tumor growth and Ki-67 observed in R3230 and MATBIII tumors post hepatic RFA ($p<0.01$). Anti-IL6 siRNA also reduced RFA-induced elevation in VEGF and tumor MVD

role in study design, data collection and analysis, decision to publish, or preparation of the manuscript.

Competing Interests: The authors have declared that no competing interests exist.

(p<0.01). Likewise, renal RFA-induced increases in serum IL-6 levels and distant R3230 tumor growth was suppressed with anti-IL6 siRNA (p<0.01).

Conclusions

Adjuvant nanoparticle-encapsulated siRNA against IL-6 can be used to modulate local and regional effects of hepatic RFA to block potential unwanted pro-oncogenic effects of hepatic or renal RFA on distant tumor.

Introduction

There has been much recent interest in using RNA interference ('post-transcriptional gene silencing') and particularly small interfering RNAs (siRNA) in cancer therapies. This has largely focused on either modulating cellular protein responses to improve efficacy of primary pharmacologic/oncologic therapies [1,2], augmenting anti-tumor immunity through selective knockdown of immune response suppressing proteins, or chemo-sensitization through silencing of growth factor receptor genes [3–6]. To overcome limitations in delivery with free siRNA in *in vivo* systems, siRNAs have been commonly administered using nanoparticle carriers (such as liposomes, micelles, or bound to particles) to maximize essentially *passive* tissue delivery (albeit in higher concentrations) to primary organs and target tumors [7–11]. Yet, even aided by nanocarrier delivery, challenges to intra-tumoral and targeted drug delivery persist [1,3]. Additionally, few studies have used adjuvant siRNA in conjunction with non-pharmacologic paradigms, such as modulating tissue or physiologic responses after surgical, interventional, or radiation treatments.

Image-guided thermal tissue ablation using radiofrequency, microwave, or laser energy to create local high temperature (60–100°C) heating around a percutaneously placed applicator is now in widespread clinical use to treat focal tumors of the liver, lung, kidney, and bone (>100,000 cases/year worldwide) [12]. Successful complete tumor ablation also requires the inclusion of a 5–10 mm rim of normal parenchyma as an 'ablative margin' to ensure complete eradication the tumor [13]. In an attempt to ensure completeness of treatment, we have shown that administration of even a single-dose of drug-loaded nanoparticle chemotherapy concurrently with RF ablation can lead to increases in local periablational drug delivery (up to 10-fold), with resultant increased tumor destruction, increased animal endpoint survival, and greater amounts of tumor destruction in patients with hepatic tumors [14–16]. Recently we have further successfully leveraged this improved focal delivery to target specific RFA-induced tissue responses (such as increased DNA intercalation or suppressing HSP production) [16,17].

A number of studies have demonstrated that sub-lethal lower tissue heating (40–47°C) around the ablation zone incites multiple secondary tissue reactions [18], including increased inflammatory cytokine (such as IL-6 and IL-10) [19] and growth factor (such as HGF, HIF-1α, and VEGF) [20–22] production; infiltration of scavenger and immunogenic cells into the periablational tissue [23]; and hyperthermia-induced increases in vascular permeability and endothelial leakiness [24]. In particular, recent studies have demonstrated that increased serum Interleukin-6 production after thermal ablation of normal liver (simulating the clinical endpoint of ablating the entire liver tumor and its 'ablative margin' of normal surrounding liver) is a key driver of periablational infiltration of inflammatory and immunogenic cells such as macrophages and α-smooth muscle actin (SMA) positive hepatic stellate cells [23,25]. These, in turn, can produce additional activation of downstream pro-growth pathways such as cytokines

in the HGF/c-Met pathway, and increased hepatocyte proliferation in untreated liver—processes which are markedly reduced in IL-6 knockout mice [25]. Given that successful complete tumor ablation also requires the inclusion of a 5–10 mm rim of normal parenchyma as an 'ablative margin' to ensure complete eradication the tumor[13], studying these secondary systemic effects of RF ablation in normal organ tissue is imperative. The need for further study is supported by recent experimental studies demonstrating, 'off-target' stimulation of distant tumor growth after thermal ablation of liver and kidney tissue, and clinical studies that suggest a higher incidence of new HCC after hepatic RF ablation (approaching 80% at 5 years) compared to comparative un-treated cirrhotic patients (22–50%)[26–29]. Here, we build on our earlier experience using nanoparticle-mediated drug delivery preferentially targeted to the periablational rim to study whether polymeric micelle-like nanoparticles (MNPs) loaded with anti-IL6 siRNA can be used to suppress thermal ablation-induced IL-6 production, IL-6-mediated periablational cell infiltration, hepatocyte proliferation in untreated liver, and IL-6-mediated downstream RF ablation-induced stimulation of distant tumor growth.

Materials and Methods

Ethics statement

All animal studies were performed with the approval of the Beth Israel Deaconess Medical Center Institutional Animal Care and Use Committee and Hadassah Hebrew University Medical School Institutional Animal Care Ethics Committee.

Animal models

For all experiments and procedures, anesthesia was induced with IP injection of a mixture of ketamine (50 mg/kg, Ketaject; Phoenix Pharmaceutical, St. Joseph, MO) and xylazine (5 mg/kg, Bayer, Shawnee Mission, KS). Animals were sacrificed with an overdose of carbon dioxide using SMARTBOX CO_2 Chamber System (EZ systems, Palmer, PA) followed by cardiac puncture.

Experiments were performed in normal C57Bl mice (40±10g), or two breast adenocarcinoma cell lines (R3230 or MATBIII) implanted subcutaneously in female Fisher 344 rats (150 ±20g; 14–16 weeks old, Charles River, Wilmington, MA) [30]. The R3230 breast adenocarcinoma tumor line is a well-characterized line that we have been using for over 10 years [30]. The MATBIII tumor line was obtained from American Type Culture Collection (ATCC, Manassas, VA). Tumor implantation, evaluation, and preparation techniques were performed as previously described [30]. Briefly, one tumor was implanted into each animal by slowly injecting 0.3–0.4 mL of tumor suspension into the mammary fat pad of each animal via an 18-gauge needle. Tumors were measured every 1-2d until they reached 6–7 mm at which point they were included in studies.

Application of RF ablation

Conventional monopolar RFA was applied by using a 500-kHz RFA generator (model 3E; Radionics, Burlington, MA), as has been previously described [30]. Briefly, the target organ was exposed via laparotomy using a subcostal (liver) or lateral (kidney) incision under sterile conditions while the animal was anesthetized. The 1-cm tip of a 21-gauge electrically insulated electrode (SMK electrode; Cosman Medical Inc, Burlington, MA) was placed in the liver or kidney. For animals treated with thermal ablation, RF energy was applied for 5 min with generator output titrated to maintain a designated tip temperature (70±2°C). This standardized method of RF application has been demonstrated previously to provide reproducible coagulation

volumes with use of this conventional RFA system [30,31]. To complete the RF circuit, the animal was placed on a standardized metallic grounding pad (Radionics). For animals treated with either sham or an agent alone, the electrode was placed, but no energy was administered.

Nanoparticle siRNA formulation

All materials were purchased from Sigma-Aldrich (St. Louis, MO) unless otherwise stated. Branched polyethylenimine (PEI) with a molecular weight of 1.8 kDa was purchased from Polysciences, Inc (Warrington, PA). 1,2-disrearoyl-sn-glycero-3-phosphoethanolamine-N-[methoxy (polyethylene glycol)-2000] (PEG-PE 2kDa) and 1,2-dioleoyl-sn-glycero-3-phosphoethanolamine-N-(glutaryl) (Glutaryl-PE) were purchased from Avanti Polar Lipids (Alabaster, AL). Nuclease-free water was purchased from Qiagen (Germantown, MD). All siRNA duplexes are from Dharmacon (Lafayette, CO). The synthesized sequences of siRNA targeting IL-6 were: 5′ -AGUCGGAGGCUUAAUUACAdTdT-3′ (sense), 5′ -CAGGAAAUUUGCCUAUUGAdTdT-3′ (sense) and 5′ -UAAGGACCAAGACCAUCCAdTdT-3′ (sense)[32,33]. A scramble siRNA was used as negative control. The sequence of non-targeting control siRNA was 5′ -AGUACUG CUUACGAUACGGdTdT-3′ (sense) [34].

Micelle-like nanoparticles were selected as the delivery vehicle based upon prior work demonstrating beneficial temporal delivery kinetics (6–12hr) and greater interstitial penetration in tissues surrounding the ablation zone [35]. We constructed micelle-like nanoparticles (MNPs) based on phospholipid modified-polyethylenimine conjugates (DOPE-PEI). The DOPE-PEI conjugate and the DOPE-PEI/siRNA complexes were prepared as previously described [34]. We have previously demonstrated that DOPE-PEI conjugates based on low molecular weight PEI self-assembled within micellar structures that condensed siRNA, showed high transfection efficiency and had a better toxicity profile than PEI 25 kDa and Lipofectamine (commonly used DNA/siRNA transfection reagents) [11]. We incorporated PEG-PE in the carriers to achieve an improved performance *in vivo*. The hydrophobic interactions between the lipid moieties in DOPE-PEI and those in PEG-PE resulted in their self-assembly into micelle-like particles with a mean size of 150 nm and provide some steric stabilization of complexes by forming a protective barrier and promoting increased stability *in vivo*. The DOPE-PEI/siRNA complexes were prepared by mixing equal volumes of DOPE-PEI with siRNA-IL-6 (equimolar pool of 3 sequences) or scramble siRNA to a final N/P ratio of 16. The siRNA solution was transferred to the polymer solution, mixed by vigorous pipetting and incubated for 15 min. The polymer/siRNA ratio was expressed as the nitrogen/phosphate (N/P) ratio, and calculated assuming that 43 g/mol corresponds to each repeating unit of PEI containing one amine and 316 g/mol corresponds to each repeating unit of siRNA containing one phosphate. Then, a previously freeze-dried lipid film of PEG-PE was hydrated with the complexes and allowed to stand at room temperature for 1h with intermittent shaking The PEG-PE2kDa:DOPE-PEI weight ratio was 2:1 [36]. Empty formulations were prepared by the hydration of the film with polymer solution only. Each mouse received a dose of 3.5 μg of siRNA in a final formulation volume of 100 μL. Each rat received a dose of 20 μg of siRNA in a final formulation volume of 200 μL. Each dose was administered by intraperitoneal injection (IP) at selected time points as specified above.

Tumor harvesting

Animals were sacrificed at specified times outlined above using carbon dioxide euthanasia. The target tissue (primary site of ablation, untreated liver lobe, or distant tumor) was harvested, and sectioned perpendicularly to the direction of electrode insertion [17,30]. Distant tumors were also harvested and sectioned. All samples were fixed in 10% formalin overnight at 4°C,

embedded in paraffin, and sectioned at a thickness of 5 μm. Tissues were stained with H&E for gross pathology.

Quantification of IL-6 and VEGF levels

Serum and tissue levels of IL-6 (Mouse/M6000B and Rat /R6000B Quantikine kit, R&D Systems Inc., Minneapolis, MN) and VEGF (Rat/RRV00 Quantikine kit, R&D Systems) were determined using an enzyme-linked immunosorbent assay (ELISA) kit according to manufacturer's instructions. Briefly, flash-frozen liver tissue was homogenized in a cold lysis buffer (Cell Signaling Technology Inc., Beverly, MA) consisting of a 0.1% proteinase inhibitor (Sigma-Aldrich). The homogenates were then centrifuged at 14,000 rpm for 20 min at 4°C, and the total protein concentration was determined using a bichinchoninic acid method (BCA) (Sigma-Aldrich). Undiluted serum was used. IL6 and VEGF values were then normalized to protein concentration. All samples and standards were measured in duplicate, and the average value was recorded as pg per mL [37,38].

Immunohistochemical staining

Sections from ablated tissue and distant tumors were prepared and immunohistochemistry staining was performed for the following markers: α-SMA (hepatic stellate cells in the periablational rim), CDC-47 (hepatocyte proliferation, untreated liver) (has been previously described (Santa Cruz Biotechnology, Dallas, TX) [17,23]), Ki-67 (ab-16667 Abcam, Cambridge, MA) (tumor cell proliferation in distant tumor), and CD34 (microvascular density in distant tumor) (AF4117 R&D systems, Minneapolis, MN). Specimen slides were imaged and analyzed using a Micromaster I microscope (Fisher Scientific, Pittsburgh, PA) and Micron Imaging Software (Westover Scientific, Inc., Mill Greek, WA). Five random high power fields were analyzed for a minimum of 3 specimens for each parameter and scored in a blinded fashion to remove observer bias [16,17]. As an additional control to insure uniformity of staining, whenever direct comparisons were made, IHC was repeated with all relevant comparison slides stained at the same time.

Statistical Analysis

The SPSS 13.0 software package (SPSS Inc., Chicago, IL) was used for statistical analysis. All data were provided as mean plus or minus SD. Selected (Day 0 and at the time of sacrifice) mean tumor sizes, and immunohistochemical quantification were compared using analysis of variance (ANOVA). Additional post-hoc analysis was performed with paired, two-tailed Student's T-test, if and only if, the analysis of variance achieved statistical significance. A P value of less than 0.05 was considered significant. Tumor growth curves after treatment were analyzed using goodness-of-fit characterization. Mean post-treatment growth curve slopes plus or minus SD were also calculated and compared using ANOVA and paired, two-tailed T-tests.

Results

Nanoparticle anti-IL6 siRNA blocks local periablational and regional distant intrahepatic effects of thermal ablation

Initial hepatic RF ablation studies were performed in normal C57Bl mice using standardized protocols to allow comparison to prior studies in normal and IL-6 knockout mice [25]. The following 6 treatment arms were compared (n = 5–6 animals/arm): hepatic RF thermal ablation alone (laparotomy and RF application for 5 min, tip temperature titrated to 70±2°C), sham procedure (laparotomy and needle placement without heating), RFA/MNP anti-IL6 siRNA

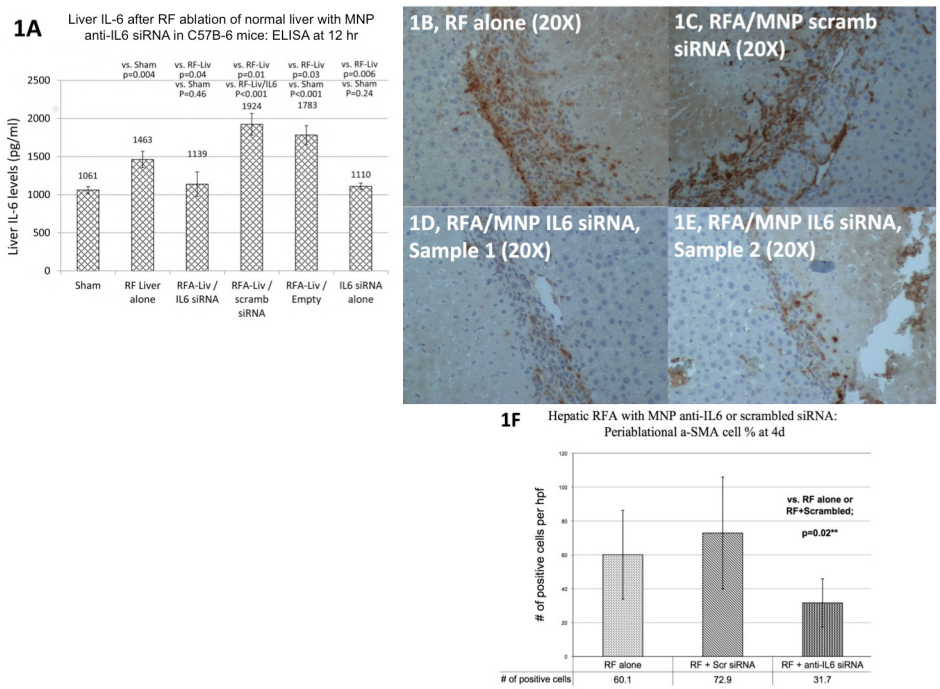

Fig 1. Hepatic thermal ablation increases liver IL-6 levels at 12hr post-treatment and periablational α-SMA+ activated myofibroblasts infiltration—which are suppressed with single dose adjuvant nanoparticle anti-IL6 siRNA. (A) Liver ELISA quantification of IL-6 levels 12hr after treatment (mean ± standard deviation). C57Bl mice were randomized to receive sham treatment, liver RF ablation, liver RFA / IP MNP anti-IL6 siRNA, MNP anti-IL6 siRNA alone, RFA / MNP scrambled siRNA, or RFA / empty carrier (n = 5–6 per group). Liver RFA increased local 12hr liver IL-6 levels (1,463±108 pg/ml) which was suppressed with adjuvant IP MNP anti-IL6 siRNA (1,139±159 pg/ml, p = 0.04). Additionally, adjuvant MNP anti-IL6 siRNA given 15 minutes after hepatic thermal ablation **(D, E)** in C57Bl mice suppressed periablational infiltration of α-SMA positive myofibroblasts compared to hepatic thermal ablation alone **(B)** or RFA combined with scrambled siRNA **(C) (F**, mean ± standard deviation, p<0.01).

doi:10.1371/journal.pone.0128910.g001

(single dose of 3.5 μg siRNA given IP, 15 min post-ablation), RFA/MNP scrambled siRNA, MNP anti-IL6 siRNA alone, RFA/empty vehicle. Hepatic RF ablation increased local periablational tissue IL-6 levels compared to sham procedure at 12hr after treatment (1,463±108pg/ml vs. 1061±45pg/ml, p = 0.004, Fig 1A). Adjuvant MNP anti-IL6 siRNA given with hepatic RFA reduced local tissue IL-6 levels (1,139±159pg/ml; p = 0.04 vs. RFA alone, p = 0.46 vs. sham). Hepatic RFA/MNP scrambled siRNA increased local tissue IL-6 levels (1,924±141pg/ml; p<0.001 vs. sham, p = 0.01 vs. RFA alone, p = <0.001 vs. RFA/anti-IL6 siRNA). Tissue IL-6 levels after MNP anti-IL6 siRNA with sham treatment was 1,110±42pg/ml, and after RFA/empty carrier was 1783±125pg/ml.

As reported previously [23], standardized RF thermal ablation of normal liver resulted in infiltration of the periablational rim by α-SMA-positive activated myofibroblasts (also known as hepatic stellate cells, a surrogate marker for the complex periablational cellular infiltration that occurs after thermal ablation) at 4 days after treatment (60.1±26.3% positive cells/hpf within the rim, Fig 1B–1E). Adjuvant MNP anti-IL6 siRNA significantly reduced α-SMA positive periablational cellular infiltration compared to other treatment arms (31.7±14.3% positive cells/hpf vs. RF alone: 60.1±26.3%; RF/scrambled siRNA: 72.9±33.0%; p<0.001; Fig 1F). Both the sham procedure alone or combined with MNP anti-IL6 siRNA alone did not result in any increase in or other changes to periablational cellular infiltration.

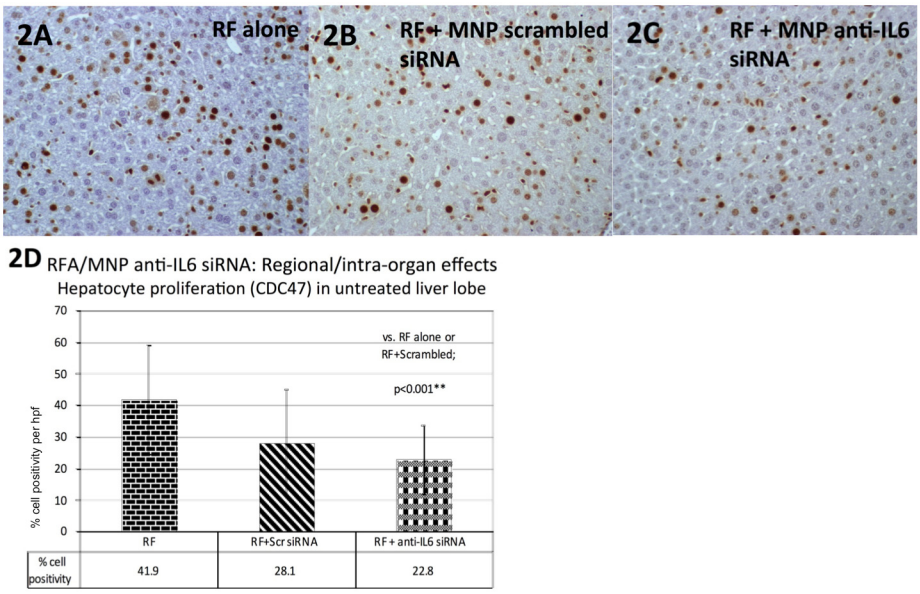

Fig 2. Adjuvant nanoparticle anti-IL6 siRNA suppresses thermal ablation-induced hepatocyte proliferation in the untreated, distant hepatic lobe. Adjuvant MNP anti-IL6 siRNA given 15 minutes after hepatic thermal ablation **(C)** in C57Bl mice (n = 5–6 animals/arm) suppressed hepatocyte proliferation in the distant, untreated liver lobe (with CDC47 staining, mean ± standard deviation) compared to hepatic thermal ablation alone **(A, D,** p<0.01). Hepatic thermal ablation combined with MNP scrambled siRNA was not significantly different from either thermal ablation alone or ablation combined with MNP anti-IL6 siRNA **(B, D)**.

doi:10.1371/journal.pone.0128910.g002

Adjuvant MNP anti-IL6 siRNA also had organ-wide effects after hepatic thermal ablation. As shown by Rozenblum et al [25], thermal ablation of one lobe of the liver increased hepatocyte proliferation in the distant, untreated liver lobe, as measured by CDC47 staining (a marker of cells entering the G1 phase of cell replication) (42.016.2% positive cells/hpf, Fig 2). MNP anti-IL6 siRNA reduced the amount of hepatocyte proliferation compared to liver thermal ablation alone (23.0±10.7%/hpf vs. 42.016.2%/hpf, $p<0.001$). No difference was observed in hepatocyte proliferation in a distant, untreated liver lobe for RFA/MNP scrambled siRNA (28.1±16.7%/hpf) compared to RF ablation alone ($p = 0.12$) or RFA/MNP anti-IL6 siRNA ($p = 0.15$) [Fig 2A–2D].

Nanoparticle anti-IL6 siRNA suppresses thermal ablation-induced stimulation of distant R3230 tumor growth and serum IL-6 levels after RF ablation of normal liver parenchyma

To determine the impact on distant tumor growth to simulate the common condition of distant metastases, we used a subcutaneous breast tumor model (R3230) in which hepatic RF ablation has been associated with distant tumor growth [26]. Here, the following treatment arms were compared (n = 6–7 animals/arm): hepatic RF thermal ablation alone, sham procedure, RFA/MNP anti-IL6 siRNA (20 mcg of siRNA, IP delivery), RFA/MNP scrambled siRNA, MNP anti-IL6 siRNA alone, RFA/empty vehicle. The effect of these six treatment arms on distant subcutaneous tumor growth was assessed. All tumors grew at the same rate over 5d prior to randomization to various treatment arms. Thermal ablation of normal liver increased distant R3230 tumor growth for 7d after treatment compared to sham/control treatment ($p<0.001$; Fig 3A, Table 1). Adjuvant MNP anti-IL6 siRNA suppressed the thermal ablation-induced effects on distant R3230 tumor growth such that the mean tumor size at 7d with

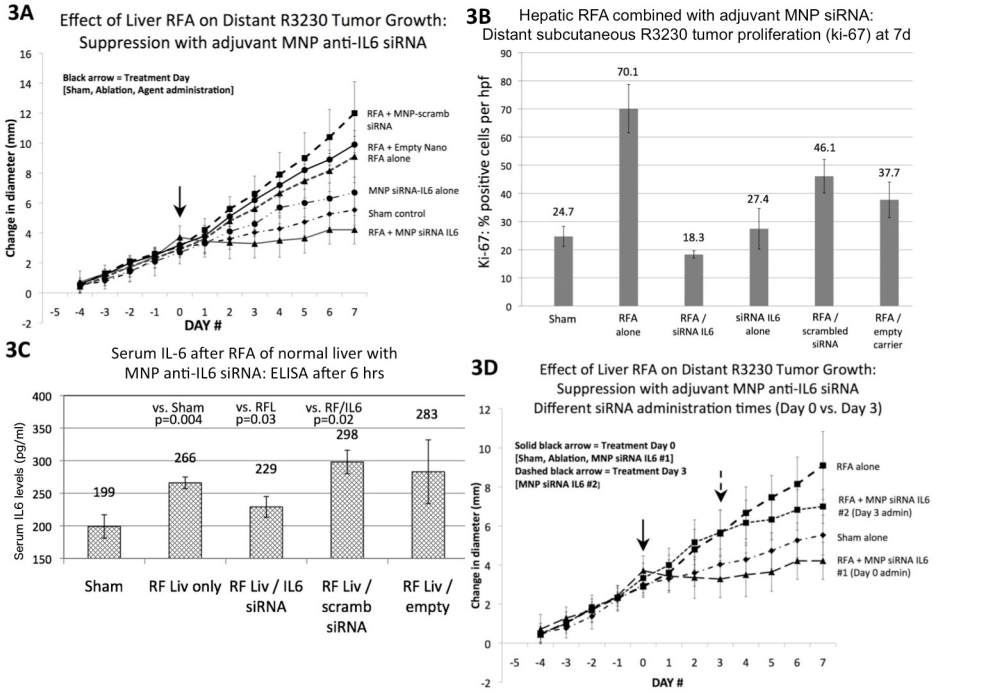

Fig 3. Hepatic thermal ablation-induced distant subcutaneous R3230 tumor growth is suppressed with adjuvant nanoparticle anti-IL6 siRNA. (A) Subcutaneous R3230 tumors implanted in Fisher 344 rats with similar growth rates were randomized at Day 0 to one of six different treatment arms (n = 6–7 animals/arm). Hepatic thermal ablation alone or combined with either empty carrier or MNP scrambled siRNA resulted in significantly greater tumor growth and change in diameter (5d before to 7d after treatment) compared to sham treatment ($p<0.01$ for all comparisons, mean ± standard deviation for all numbers presented). Adjuvant MNP anti-IL6 siRNA combined with thermal ablation resulted in distant tumor growth rate and end diameter that was the lowest of all treatment arms ($p<0.01$ for all comparisons). **(B)** Adjuvant MNP anti-IL6 siRNA combined with hepatic thermal ablation also reduced distant tumor proliferation (Ki-67) to sham levels compared to hepatic thermal ablation alone or combined with empty carrier or MNP scrambled siRNA ($p<0.01$ for relevant comparisons). **(C)** Hepatic thermal ablation alone or with MNP scrambled siRNA increased serum IL-6 levels at 6hr compared to the sham procedure (n = 3–4 animals/arm, $p<0.02$). This effect was suppressed with adjuvant MNP anti-IL6 siRNA ($p = 0.03$ vs. RF liver alone). **(D)** Comparison of the effect of siRNA administration timing showed that adjuvant MNP anti-IL6 siRNA administered at Day 0 resulted in the lowest post-treatment tumor growth rate and endpoint diameter (n = 3–4 animals/arm, $p<0.05$ for all comparisons). Adjuvant MNP anti-IL6 siRNA administered 3d post-ablation reduced the endpoint diameter compared to hepatic ablation alone, but was still significantly greater that either sham or combined-Day 0 treatment ($p<0.05$ for all comparisons).

doi:10.1371/journal.pone.0128910.g003

combination therapy was lower than either the sham (non-ablation) and hepatic RFA alone groups ($p = 0.02$ vs. sham, $p<0.001$ vs. hepatic RFA alone; Fig 3A, Table 1). Hepatic RF ablation combined with MNP scrambled siRNA resulted in the largest distant tumor diameter at 7d compared to all other treatment arms (19.3±1.7mm, $p<0.03$ for all comparisons).

Tumor proliferative index (Ki-67) in the distant R3230 subcutaneous tumor was measured for all treatment arms [Fig 3B, Table 1]. Hepatic thermal ablation increased distant tumor proliferation at 7d compared to the sham procedure ($p = 0.001$). Combination adjuvant MNP anti-IL6 siRNA and hepatic thermal ablation significantly reduced distant tumor proliferation ($p = 0.045$ vs. sham, $p<0.001$ vs. hepatic RFA alone). Thermal ablation combined with either empty carrier or MNP scrambled siRNA resulted in increased distant tumor prolilferation ($p<0.04$ compared to sham treatment). There was no difference between sham treatment and MNP anti-IL6 siRNA alone arms ($p = 0.59$).

Table 1. Evaluation of distant tumor after thermal ablation without and with adjuvant MNP siRNA.

Treatment arms	End tumor diameter (mm)	Change in diameter after treatment(mm)	Pre Growth Curve Slope	Post Growth Curve Slope	Tumor Ki-67 (% cell positivity/hpf)	MVD / CD34 (vessel # per hpf)
LIVER thermal ablation without and with anti-IL6 siRNA on distant R3230 tumor growth (7d)						
Sham treatment	13.8 ± 0.8	5.7 ± 1.1	0.64 ± 0.12	0.37 ± 0.16	24.7 ± 3.6	25.1 ± 8.1
RFA liver alone	17.0 ± 2.0	9.1 ± 1.7	0.62 ± 0.08	0.89 ± 0.24	70.1 ± 8.6	50.9 ± 15.9
RFA liver + anti-IL6 siRNA (given at Day 0)	12.6 ± 1.5	4.2 ± 1.0	0.75 ± 0.50	0.20 ± 0.01	18.3 ± 1.4	22.9 ± 3.2
anti-IL6 siRNA alone	14.7 ± 1.0	6.7 ± 1.0	0.59 ± 0.21	0.59 ± 0.18	27.4 ± 7.2	29.1 ± 1.0
RFA liver + scramb siRNA	19.3 ± 1.7	12.0 ± 2.1	0.65 ± 0.11	1.25 ± 0.30	37.8 ± 6.3	56.3 ± 3.1
RFA liver + empty carrier	17.1 ± 0.4	9.9 ± 0.5	0.65 ± 0.12	0.99 ± 0.09	46.1 ± 6.0	49.3 ± 7.8
RFA liver + anti-IL6 siRNA (given at Day 3)	15.5 ± 1.0	7.0 ± 0.9	0.85 ± 0.21	0.55 ± 0.49	28.2 ± 1.5	30.6 ± 2.8
KIDNEY thermal ablation without and with anti-IL6 siRNA on distant R3230 tumor growth (7d)						
Sham treatment	14.5 ± 1.2	6.4 ± 0.7	0.65 ± 0.11	0.45 ± 0.08	15.5 ± 5.6	16.9 ± 2.3
RFA kidney alone	19.6 ± 1.8	11.2 ± 1.5	0.61 ± 0.07	1.18 ± 0.26	45.1 ± 4.3	33.1 ± 4.4
RFA kidney + anti-IL6 siRNA	13.9 ± 1.2	5.7 ± 1.2	0.64 ± 0.22	0.35 ± 0.16	19.4 ± 2.0	19.6 ± 0.5
Anti-IL6 siRNA alone	15.7 ± 0.3	7.0 ± 0.9	0.75 ± 0.15	0.50 ± 0.16	28.4 ± 3.6	26.4 ± 0.9
LIVER thermal ablation without and with anti-IL6 siRNA in a SECOND TUMOR (MATBIII) (3.5d)						
Sham treatment	21.9 ± 1.2	11.4 ± 1.5	1.83 ± 0.21	0.39 ± 0.20	57.5 ± 7.7	32.8 ±7.9
RFA liver alone	24.4 ± 2.5	14.7 ± 2.0	1.86 ± 0.44	0.77 ± 0.20	75.8 ± 1.7	49.9 ± 7.3
RFA liver + anti-IL6 siRNA	20.6 ± 1.7	11.5 ± 1.0	1.80 ± 0.14	0.27 ± 0.22	44.8 ± 6.9	15.9 ± 0.9

All numbers provided as mean ± standard deviation.

doi:10.1371/journal.pone.0128910.t001

Next, serum IL-6 levels were quantified by ELISA at 6hr after treatment for each of the six arms (n = 3–4 animals/arm) to determine the effect of adjuvant MNP anti-IL6 siRNA on ablation-induced systemic IL-6 levels. This time point was selected as serum IL-6 levels peaked at 6hr in this model post-hepatic RFA. Serum IL-6 levels were increased after thermal hepatic ablation (266±9pg/ml) compared to sham treatment (199±18pg/ml, p = 0.005) [Fig 3C]. The addition of MNP anti-IL6 siRNA reduced serum IL6 levels at 6hr (229±16pg/ml) compared to RFA alone (p = 0.03) or RFA/MNP scrambled siRNA (298±18pg/ml, p = 0.02). RFA/empty carrier also increased serum IL6 levels at 6hrs similar to RFA alone (298±18pg/ml, p = 0.57).

Finally, timing of siRNA administration was compared, and MNP anti-IL6 siRNA administered immediately after hepatic RFA (Day 0) resulted in complete suppression of RFA-induced tumor growth compared to administration at a later time point (3d) after hepatic RFA (Day 0 vs. Day 3, $p<0.02$) [Fig 3D, Table 1]. Similarly, for the hepatic RFA / nano anti-IL6 siRNA at Day 0, the tumor proliferative index at 7d was significantly lower compared to Day 3 administration (p = 0.001).

Nanoparticle anti-IL6 siRNA suppresses hepatic ablation-induced distant tumor growth through reduction in VEGF-mediated tumor angiogenesis

Periablational liver tissue levels of VEGF were increased after thermal ablation, peaking at 72hr. Here, tissue VEGF levels in the periablational rim were compared using ELISA at 72hr after treatment for the following arms: hepatic RF thermal ablation alone, sham procedure,

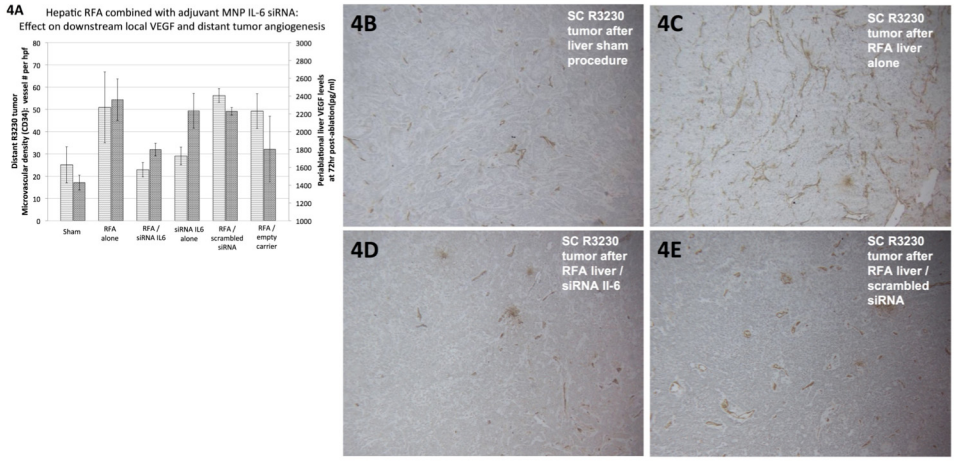

Fig 4. Adjuvant nanoparticle anti-IL6 siRNA suppresses hepatic ablation-induced distant subcutaneous R3230 tumor growth via reduction in VEGF-mediated angiogenesis. (A) Tissue levels of VEGF (Y-axis[2], dark gray columns) in the periablational tissue surrounding the ablation zone were quantified at 72hr after different treatments (mean ± standard deviation, n = 3–4 animals/arm). Hepatic thermal ablation increased periablational VEGF levels, which were then suppressed with adjuvant MNP anti-IL6 siRNA ($p<0.05$ for all comparisons). **(B-E)** Similarly, hepatic thermal ablation led to increased microvascular density/ angiogenesis (immunohistochemistry for CD34, A: Y-axis[1], light gray columns) in distant subcutaneous R3230 tumor that was also suppressed with adjuvant anti-IL6 siRNA (n = 6–7 animals/arm).

doi:10.1371/journal.pone.0128910.g004

RFA/MNP anti-IL6 siRNA (20g of siRNA, IP delivery), RFA/MNP scrambled siRNA, MNP anti-IL6 siRNA alone, RFA/empty vehicle (n = 3–4 animals/arm). Hepatic ablation increased periablational tissue VEGF levels compared to sham treatment at 72hr (2359±233pg/ml vs. 1429±83pg/ml, p = 0.002) [Fig 4A]. Adjuvant MNP anti-IL6 siRNA reduced liver VEGF levels after thermal ablation (1799±71pg/ml, p = 0.02 vs. ablation). Hepatic ablation combined with adjuvant scrambled siRNA led to similar liver VEGF levels compared to RFA alone (2229 ±42pg/ml; vs. RFA alone: p = 0.51; vs. sham: p = 0.001). No difference was observed for thermal ablation combined with the empty carrier compared to other treatment arms (1804±370pg/ml; vs. RFA alone: p = 0.09; vs. sham: p = 0.16). MNP anti-IL6 siRNA alone had greater liver tissue VEGF levels compared to sham (2234±195pg/ml, p = 0.002).

Microvascular density (using CD34 staining) was then compared in distant subcutaneous tumors for each of the six treatment arms at 7d post-treatment [Fig 4B–4E, Table 1]. Hepatic thermal ablation increased distant tumor microvascular density at 7d compared to the sham procedure (p = 0.003). Combination adjuvant MNP anti-IL6 siRNA and hepatic thermal ablation significantly reduced distant tumor microvascular density (p = 0.01 vs. hepatic RFA alone). Thermal ablation combined with either empty carrier or scrambled siRNA resulted in increased distant tumor microvascular density ($p<0.003$ compared to sham treatment). There was no difference between sham treatment and MNP anti-IL6 siRNA alone arms (p = 0.46). These findings suggest that blocking of hepatic ablation-induced distant tumor growth by adjuvant anti-IL6 siRNA is mediated by suppression of downstream VEGF production and distant tumor angiogenesis.

Nanoparticle anti-IL6 siRNA suppresses distant tumor growth after RF ablation in a second primary organ site (normal kidney)

For tumor growth studies, kidney RF thermal ablation alone, sham procedure, RFA/MNP anti-IL6 siRNA (20g of siRNA, IP delivery), and MNP anti-IL6 siRNA alone were compared

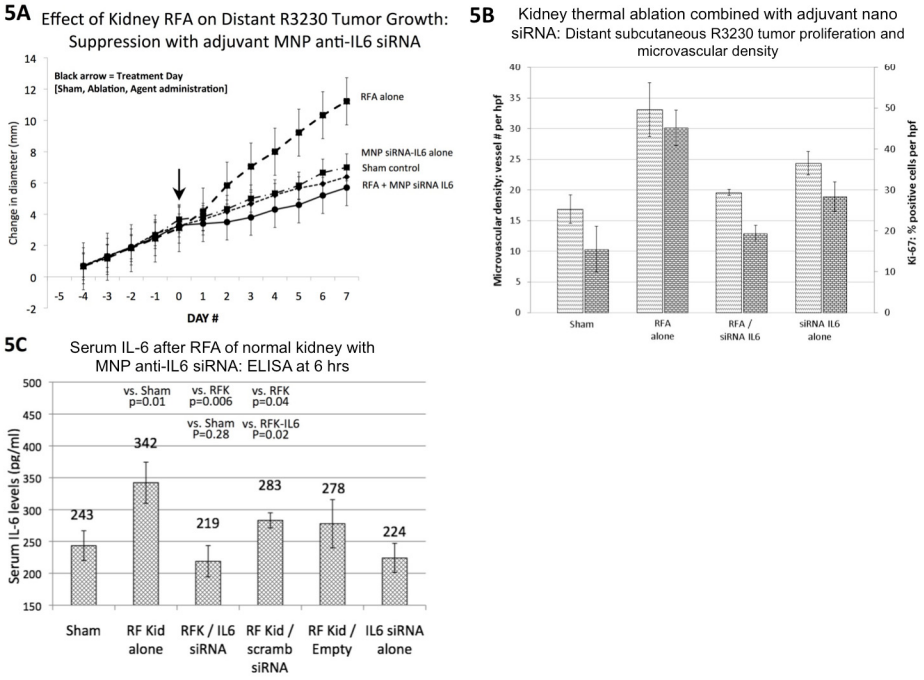

Fig 5. Thermal ablation of a second primary organ (kidney) leads to increased distant subcutaneous R3230 tumor growth that is suppressed with adjuvant nanoparticle anti-IL6 siRNA. (A) Subcutaneous R3230 tumors implanted in Fisher 344 rats with similar growth rates were randomized at Day 0 to one of four different treatment arms (n = 6–7 animals/arm). Thermal ablation of normal kidney alone resulted in significantly greater tumor growth and change in diameter (5d before to 7d after treatment) compared to sham treatment or MNP anti-IL6 siRNA alone ($p<0.01$ for all comparisons, mean ± standard deviation for all data). MNP anti-IL6 siRNA combined with thermal ablation reduced distant tumor growth rate and endpoint diameter to baseline sham levels. **(B)** Adjuvant MNP anti-IL6 siRNA combined with kidney thermal ablation also reduced distant tumor proliferation (Ki-67) and microvascular density (CD34) to baseline levels compared to kidney thermal ablation alone ($p<0.01$ for relevant comparisons). **(C)** Adjuvant MNP anti-IL6 siRNA suppressed kidney thermal ablation-induced elevations in serum IL-6 levels at 6hr post-treatment (n = 3–4 animals/arm, p = 0.006).

doi:10.1371/journal.pone.0128910.g005

(n = 6–7 animals/arm). Similarly, RF ablation of normal kidney increased distant R3230 tumor growth compared to sham treatment that was also suppressed with single-dose adjuvant MNP anti-IL6 siRNA (given at Day 0) [Fig 5A, Table 1]. Tumor proliferative index and microvascular density for combination nanoparticle anti-IL6 and sham arms were equivalent to each other and lower compared to the group treated with RF ablation of normal kidney alone [Fig 5B, Table 1].

Next, serum IL6 levels were studied in the following treatment arms: kidney RF thermal ablation alone, sham procedure, RFA/MNP anti-IL6 siRNA (20g of siRNA, IP delivery), RFA/MNP scrambled siRNA, MNP anti-IL6 siRNA alone, RFA/empty vehicle (n = 3–4 animals/arm). Serum IL-6 levels (quantified by ELISA 6hr after thermal ablation) were increased after kidney thermal ablation (342±32pg/ml) compared to sham treatment (243±23pg/ml, p = 0.005) [Fig 5C]. The addition of MNP anti-IL6 siRNA reduced serum IL6 levels at 6hr (219 ±25pg/ml) compared to RFA alone (p = 0.03) or RFA/MNP scrambled siRNA (283±12pg/ml, p = 0.02). RFA/empty carrier also increased serum IL6 levels at 6hr similar to RFA alone (278 ±38pg/ml, p = 0.57).

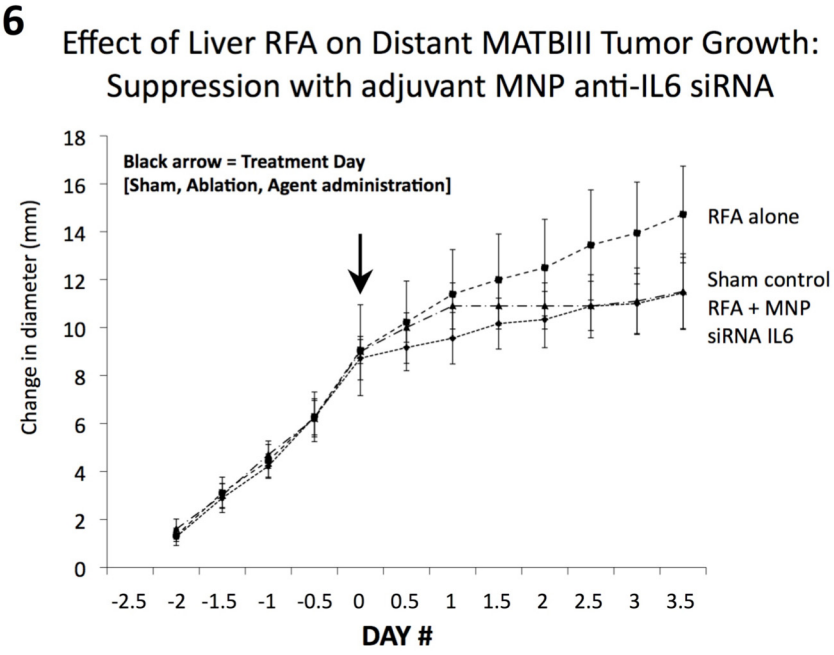

Fig 6. Hepatic thermal ablation-induced distant tumor growth is suppressed with adjuvant nanoparticle anti-IL6 siRNA in a second breast adenocarcinoma tumor model (MATBIII). Subcutaneous MATBIII tumors implanted in Fisher 344 rats with similar growth rates were randomized at Day 0 to one of three different treatment arms (sham treatment and hepatic RF ablation without and with adjuvant IP MNP anti-IL6 siRNA; n = 6–7 animals/arm). Given the rapid growth rate of this line, tumors were measured twice daily 2.5d pre- to 3.5d post-treatment (mean ± standard deviation). Hepatic thermal ablation resulted in a significantly larger endpoint tumor diameter compared to the sham group ($p<0.05$). Adjuvant MNP anti-IL6 siRNA suppressed the effects of hepatic thermal ablation, such that endpoint tumor diameter was equivalent to the sham group.

doi:10.1371/journal.pone.0128910.g006

Nanoparticle anti-IL6 siRNA suppresses distant tumor growth in a second tumor model (MATBIII) after hepatic thermal ablation

Next, the effect of MNP anti-IL6 siRNA on hepatic thermal ablation was assessed in a second subcutaneous tumor model (MATBIII rat breast adenocarcinoma line) at 3.5d post-treatment (due to the relatively faster innate tumor growth rate, all tumors reached the mandated size for sacrifice after 3.5d) [Table 1]. Hepatic thermal ablation without and with adjuvant IP MNP anti-IL6 siRNA was compared to sham treatment (n = 6–7 animals/arm). All tumors grew at the same rate over 2.5d prior to randomization to treatment. Hepatic thermal ablation again resulted in significantly larger distant subcutaneous MATBIII tumors at 3.5d compared to the sham procedure ($p = 0.001$, Fig 6). Adjuvant MNP anti-IL6 siRNA post-ablation reduced the tumor growth rate such that endpoint diameter was significantly smaller than hepatic ablation alone, and equal to the sham arm (vs. RFA alone $p = 0.009$, vs. sham $p = 0.94$, Table 1). RFA alone also resulted in significantly greater cellular proliferation and microvascular density in the distant MATBIII tumor compared to RFA with MNP anti-IL6 siRNA or sham treatment ($p<0.05$ for all comparisons, Table 1).

Discussion

Several studies have reported that incomplete thermal tumor ablation of intrahepatic or renal tumors can have either stimulatory or suppressive effects on tumor cell growth in the partially

injured residual cells present in periablational tissue or in intrahepatic/intra-organ tumor foci separate from the ablation site [21,22,39,40]. For example, Nijkamp et al. reported increases in periablative tumor outgrowth after incomplete ablation of murine intrahepatic colorectal metastases [21]. Regardless, potential RF ablation-induced stimulation of distant extrahepatic tumor growth remains poorly characterized. Here, we confirm recent reports that thermal ablation of normal organ parenchyma (such as liver or kidney) can stimulate distant tumor growth in at least two different tumor models [27], and further demonstrate that this in part due to ablation-induced increases in IL-6. Ultimately, this is potentially very clinically relevant, as the standard clinical endpoint in widespread practice is to ablate the entire tumor and up to a 5–10 mm circumferential margin of normal parenchymal tissue around the ablation zone [41]. Additionally, thermal ablation is increasingly applied as the primary treatment of oligometastatic disease, as part of multi-modality treatments where other existing tumors are being treated differently, or to target active metastatic foci in combination with systemic chemotherapy—all circumstances where small viable tumor cells are likely present separate from the ablation zone [42–44]. Therefore, for virtually all clinical cases of successful thermal tumor ablation, the potential for stimulation of tumor foci elsewhere in the body exists.

Our study further demonstrates that adjuvant nanoparticle siRNA can be successfully used to target IL-6 mediated locoregional and systemic effects of thermal ablation. Specifically, adjuvant siRNA can be used to suppress thermal ablation-induced increases in local and serum IL-6 cytokine levels, alter cellular infiltration patterns surrounding local thermal ablation, affect liver physiology/homeostasis by reducing ablation-induced hepatocyte proliferation in untreated liver, and achieve systemic suppression of un-intended 'off-target' distant pro-oncogenic effects of thermal ablation. Furthermore, we demonstrate that these RF-induced effects occur in various settings (here, in two tumor models, two organs, and two species), are IL6-mediated in these scenarios, and most importantly that they can be reproducibly modulated and attenuated with nano-delivered siRNA.

Thermal ablation incites several additional local tissue reactions, including increased oxidative and nitrative stress-mediated apoptosis and production of local tissue factors such as heat shock proteins, hepatocyte growth factor, and pro-angiogenic VEGF, HIF-1α, and PDGF [14,18,21,22]. Here, we also show that suppressing IL-6 with adjuvant siRNA blocks downstream production of VEGF and distant tumor angiogenesis, underscoring the potential utility of using adjuvant siRNA when the target is sufficiently upstream in the pathway. Additionally, while several of these pathways are linked to IL-6, those that are not could also potentially be targeted using other siRNAs to suppress production of alternative key proteins/mediators.

Our successful 'proof-of-concept' study demonstrates that nano-delivered siRNA can be used to suppress the secondary local and systemic 'off-target' effects (such as IL6-mediated inflammation) occurring after at least one clinically common procedure. Yet, there is also broader potential clinical applicability of this approach, as thermal ablative techniques have been incorporated into the treatment of a large number of diseases, including therapies such as pulmonary vein ablation for cardiac arrhythmias, esophageal ablation of Barrett's esophagus, and in newer endovascular treatments for renovascular hypertension, mitral regurgitation, vascular stenosis, and venous reflux disease [45–48]. For several of these, secondary systemic inflammatory reactions (mediated by cytokines such as IL-6, C-reactive protein, and tumor necrosis factor) have been linked to treatment failure [49,50], and have been the basis for the incorporation of adjuvant peri-procedural anti-inflammatory drug therapies [51,52].

One of the main limitations of transitioning siRNA to therapeutic applications has been due to challenges in drug-delivery [53]. In particular, free siRNA has a very short blood circulating half-life (on the order of minutes to an hour), making target-site accumulation a critical barrier to siRNA efficacy [1,54]. Nanocarrier delivery has been one strategy studied to overcome

obstacles of targeted delivery and extracellular siRNA breakdown by facilitating direct internalization through membrane fusion [55]. We have previously shown that nanocarriers preferentially accumulate around in the rim of tissue immediately surrounding the ablation zone due to heat-induced increases in vasodilation and endothelial leakiness [14,24,31]. Here, we show that thermal tissue ablation and nanocarrier anti-IL6 siRNA are particularly complementary as we take advantage of the fact that heating-induced vascular permeability occurs in the same geographic tissue region where infiltrating cells and increased IL-6 production is taking place, resulting in sufficiently high concentrations of anti-IL6 siRNA to render it effective in altering the cellular milieu and its composition. Given the predicTable and significant increases in nanoparticle delivery that can be achieved around tissue ablation or with targeted low-level hyperthermia, this combination strategy could potentially be used to facilitate siRNA delivery for other diseases that do not specifically require tissue heating but may benefit from higher levels of interstitial siRNA delivery. In addition to increased targeting specificity, additional advantages of this combination paradigm concentrating siRNA near cells that are the intended target (and conversely, minimizing exposure to non-target 'normal' cells), and increasing silencing potency by achieving higher local delivery.

We acknowledge several limitations in this study. Although we have focused on the pro-oncogenic effects of tumor ablation-induced inflammation, several studies have reported upon the potential for ablation-induced anti-tumor immunity (either alone or in combination with immunomodulation) with resultant tumor growth suppression [39,56–58]. While immunogenic effects of hepatic RF ablation are beyond the scope of this study, clearly additional research is required to understand the activating factors and balance between these two opposing effects. Thus, further translational study is envisioned defining the relevance of IL-6 and VEGF siRNA to other tumor types (including those with variable growth rates) and organs commonly ablated in clinical practice which may be more or less expressive of these cytokines. Indeed, given the host of reactions that have been identified in the periablational rim thus far, it is also likely that a number of other mediators are up-regulated (potentially downstream as part of the pathway studied here, or as a parallel pathway), such as other mediators of inflammation, the HGF/c-Met pathway, and downstream intracellular activators (such as PI3/Akt or STAT3 pathways). Several of these may also be potential therapeutic targets that merit further study. Along these lines, while we have studied radiofrequency-based thermal ablation (as this is the most commonly used modality in clinical practice), additional study will be required to determine the extent of applicability of our findings to other methods of ablation including, cryoablation, microwave thermal ablation, and irreversible electroporation[12]. Indeed, even higher post-treatment IL-6 levels have been reported for some therapies, such as cryoablation, compared to RF ablation [19]. Finally, it is possible that administration of the adjuvant drug, either through siRNA alone, interaction of lipid carrier components in the periablational rim, or the act of intraperitoneal administration also contributes to the inflammatory response. Indeed, we have previously shown that lipid components of the nanoparticle can be active independent from the drug payload [59]. Similarly, siRNA can induce a reactive inflammatory response [60], which likely explains the marginally higher distant tumor growth rate in the scrambled siRNA treatment arm (where there are no suppressive effects of the anti-IL6 siRNA) compared to even RF ablation alone. However, ultimately, the use of adjuvant anti-IL6 siRNA with RF ablation effectively suppresses any additional increases in inflammation associated with its administration.

In conclusion, we demonstrate that thermal ablation of normal organ parenchyma (such as is required in clinical practice) can result in Interleukin-6-mediated locoregional and systemic effects (including distant tumor growth). We further show that the novel paradigm of

combining adjuvant nanoparticle anti-IL6 siRNA can be successfully used to suppress potentially pro-oncogenic effects of thermal ablation.

Author Contributions

Conceived and designed the experiments: MA GK GN YW SG MHM NR TL EG VPT SNG. Performed the experiments: MA GK GN YW SG MHM NR SNG. Analyzed the data: MA GK GN YW SG MHM NR TL EG VPT SNG. Contributed reagents/materials/analysis tools: MA GK GN YW SG MHM NR TL EG VPT SNG. Wrote the paper: MA GK GN YW SG MHM NR TL EG VPT SNG.

References

1. Kanasty R, Dorkin JR, Vegas A, Anderson D. Delivery materials for siRNA therapeutics. Nature materials. 2013 Nov; 12(11):967–77. PMID: 24150415. doi: 10.1038/nmat3765
2. Resnier P, Montier T, Mathieu V, Benoit JP, Passirani C. A review of the current status of siRNA nanomedicines in the treatment of cancer. Biomaterials. 2013 Sep; 34(27):6429–43. PMID: 23727262. doi: 10.1016/j.biomaterials.2013.04.060
3. Gavrilov K, Saltzman WM. Therapeutic siRNA: principles, challenges, and strategies. The Yale journal of biology and medicine. 2012 Jun; 85(2):187–200. PMID: 22737048. Pubmed Central PMCID: 3375670.
4. Mao CP, Hung CF, Wu TC. Immunotherapeutic strategies employing RNA interference technology for the control of cancers. Journal of biomedical science. 2007 Jan; 14(1):15–29. PMID: 17103251.
5. Niu J, Li XN, Qian H, Han Z. siRNA mediated the type 1 insulin-like growth factor receptor and epidermal growth factor receptor silencing induces chemosensitization of liver cancer cells. Journal of cancer research and clinical oncology. 2008 Apr; 134(4):503–13. PMID: 17901981.
6. Thiel KW, Hernandez LI, Dassie JP, Thiel WH, Liu X, Stockdale KR, et al. Delivery of chemo-sensitizing siRNAs to HER2+-breast cancer cells using RNA aptamers. Nucleic acids research. 2012 Jul; 40 (13):6319–37. PMID: 22467215. Pubmed Central PMCID: 3401474. doi: 10.1093/nar/gks294
7. de Martimprey H, Vauthier C, Malvy C, Couvreur P. Polymer nanocarriers for the delivery of small fragments of nucleic acids: oligonucleotides and siRNA. European journal of pharmaceutics and biopharmaceutics: official journal of Arbeitsgemeinschaft fur Pharmazeutische Verfahrenstechnik eV. 2009 Mar; 71(3):490–504. PMID: 18977435.
8. Jeong JH, Mok H, Oh YK, Park TG. siRNA conjugate delivery systems. Bioconjugate chemistry. 2009 Jan; 20(1):5–14. PMID: 19053311. doi: 10.1021/bc800278e
9. Oh YK, Park TG. siRNA delivery systems for cancer treatment. Advanced drug delivery reviews. 2009 Aug 10; 61(10):850–62. PMID: 19422869. doi: 10.1016/j.addr.2009.04.018
10. Dong Y, Love KT, Dorkin JR, Sirirungruang S, Zhang Y, Chen D, et al. Lipopeptide nanoparticles for potent and selective siRNA delivery in rodents and nonhuman primates. Proceedings of the National Academy of Sciences of the United States of America. 2014; 111(11):3955–60. PMID: 24516150. doi: 10.1073/pnas.1322937111
11. Navarro G, Essex S, Sawant RR, Biswas S, Nagesha D, Sridhar S, et al. Phospholipid-modified polyethylenimine-based nanopreparations for siRNA-mediated gene silencing: Implications for transfection and the role of lipid components. Nanomedicine: nanotechnology, biology, and medicine. 2013; 10 (2):411–9. PMID: 23928214.
12. Ahmed M, Brace CL, Lee FT Jr, Goldberg SN. Principles of and advances in percutaneous ablation. Radiology. 2011 Feb; 258(2):351–69. PMID: 21273519. doi: 10.1148/radiol.10081634
13. Wang X, Sofocleous CT, Erinjeri JP, Petre EN, Gonen M, Do KG, et al. Margin size is an independent predictor of local tumor progression after ablation of colon cancer liver metastases. Cardiovascular and interventional radiology. 2013 Feb; 36(1):166–75. PMID: 22535243. doi: 10.1007/s00270-012-0377-1
14. Ahmed M, Moussa M, Goldberg SN. Synergy in cancer treatment between liposomal chemotherapeutics and thermal ablation. Chem Phys Lipids. 2012; 165(4):424–37. PMID: 22197685. doi: 10.1016/j.chemphyslip.2011.12.002
15. Wood BJ, Poon RT, Locklin JK, Dreher MR, Ng KK, Eugeni M, et al. Phase I study of heat-deployed liposomal doxorubicin during radiofrequency ablation for hepatic malignancies. J Vasc Interv Radiol. 2012 Feb; 23(2):248–55 e7. PMID: 22178041. Pubmed Central PMCID: 3264789. doi: 10.1016/j.jvir.2011.10.018

16. Yang W, Ahmed M, Tasawwar B, Levchenko T, Sawant RR, Collins M, et al. Radiofrequency ablation combined with liposomal quercetin to increase tumour destruction by modulation of heat shock protein production in a small animal model. Int J Hyperthermia. 2011; 27(6):527–38. PMID: 21846189. Pubmed Central PMCID: 3417059. doi: 10.3109/02656736.2011.582474

17. Solazzo SA, Ahmed M, Schor-Bardach R, Yang W, Girnun GD, Rahmanuddin S, et al. Liposomal doxorubicin increases radiofrequency ablation-induced tumor destruction by increasing cellular oxidative and nitrative stress and accelerating apoptotic pathways. Radiology. 2010 Apr; 255(1):62–74. PMID: 20160000. Pubmed Central PMCID: 2843831. doi: 10.1148/radiol.09091196

18. Chu KF, Dupuy DE. Thermal ablation of tumours: biological mechanisms and advances in therapy. Nature reviews Cancer. 2014 Mar; 14(3):199–208. PMID: 24561446. doi: 10.1038/nrc3672

19. Erinjeri JP, Thomas CT, Samoilia A, Fleisher M, Gonen M, Sofocleous CT, et al. Image-guided Thermal Ablation of Tumors Increases the Plasma Level of Interleukin-6 and Interleukin-10. J Vasc Interv Radiol. 2013 Aug; 24(8):1105–12. PMID: 23582441. doi: 10.1016/j.jvir.2013.02.015

20. Kong J, Kong J, Pan B, Ke S, Dong S, Li X, et al. Insufficient radiofrequency ablation promotes angiogenesis of residual hepatocellular carcinoma via HIF-1alpha/VEGFA. PLoS One. 2012; 7(5):e37266. PMID: 22615958. doi: 10.1371/journal.pone.0037266

21. Nijkamp MW, van der Bilt JD, de Bruijn MT, Molenaar IQ, Voest EE, van Diest PJ, et al. Accelerated perinecrotic outgrowth of colorectal liver metastases following radiofrequency ablation is a hypoxia-driven phenomenon. Ann Surg. 2009 May; 249(5):814–23. PMID: 19387320. doi: 10.1097/SLA.0b013e3181a38ef5

22. Nikfarjam M, Muralidharan V, Christophi C. Altered growth patterns of colorectal liver metastases after thermal ablation. Surgery. 2006 Jan; 139(1):73–81. PMID: 16364720.

23. Rozenblum N, Galun E, Zeira E, Nissenbaum I, Goldberg SN. Cellular Kinetics Following Radiofrequency (RF) Ablation in the Liver Radiological Society of North America, Proceedings of Annual Meeting. 2011:70.

24. Kruskal JB, Oliver B, Huertas JC, Goldberg SN. Dynamic intrahepatic flow and cellular alterations during radiofrequency ablation of liver tissue in mice. J Vasc Interv Radiol. 2001 Oct; 12(10):1193–201. PMID: 11585886.

25. Rozenblum N, Zeira E, Bulvik B, Gourevitch S, Yotvat H, Galun E, et al. Inflammatory changes in the peri-ablative zone following radiofrequency ablation can induce global organ effects including liver regeneration. Radiology. 2014;[in press].

26. Ahmed M, Kumar G, Moussa M, Rozenblum N, Goldberg SN. Radiofrequency (RF) ablation of normal liver increases tumor growth of remote subcutaneous tumors in an animal tumor model. J Vasc Interv Radiol. 2013; 24(4):S44.

27. Kumar G, Goldberg SN, Moussa M, Rozenblum N, Ahmed M. Radiofrequency (RF) Ablation: Does the Primary Site of Ablation Affect Distant Tumor Growth? Radiological Society of North America; Proceedings of Annual Meeting. 2013:77.

28. Lencioni R, Cioni D, Crocetti L, Franchini C, Pina CD, Lera J, et al. Early-stage hepatocellular carcinoma in patients with cirrhosis: long-term results of percutaneous image-guided radiofrequency ablation. Radiology. 2005 Mar; 234(3):961–7. PMID: 15665226.

29. Mittal S, El-Serag HB. Epidemiology of hepatocellular carcinoma: consider the population. Journal of clinical gastroenterology. 2013 Jul; 47 Suppl:S2–6. PMID: 23632345. Pubmed Central PMCID: 3683119. doi: 10.1097/MCG.0b013e3182872f29

30. Ahmed M, Monsky WE, Girnun G, Lukyanov A, D'Ippolito G, Kruskal JB, et al. Radiofrequency thermal ablation sharply increases intratumoral liposomal doxorubicin accumulation and tumor coagulation. Cancer Res. 2003 Oct 1; 63(19):6327–33. PMID: 14559820.

31. Monsky WL, Kruskal JB, Lukyanov AN, Girnun GD, Ahmed M, Gazelle GS, et al. Radio-frequency ablation increases intratumoral liposomal doxorubicin accumulation in a rat breast tumor model. Radiology. 2002 Sep; 224(3):823–9. PMID: 12202721.

32. Mostafa Anower AK, Shim JA, Choi B, Sohn S. Pretreatment with interleukin-6 small interfering RNA can improve the survival rate of polymicrobial cecal ligation and puncture mice by down regulating interleukin-6 production. European journal of pharmacology. 2012 Aug 5; 688(1–3):76–83. PMID: 22634167. doi: 10.1016/j.ejphar.2012.05.007

33. Shim J, Byun HO, Lee YD, Lee ES, Sohn S. Interleukin-6 small interfering RNA improved the herpes simplex virus-induced systemic inflammation in vivo Behcet's disease-like mouse model. Gene therapy. 2009 Mar; 16(3):415–25. PMID: 19092856. doi: 10.1038/gt.2008.180

34. Navarro G, Sawant RR, Biswas S, Essex S, Tros de Ilarduya C, Torchilin VP. P-glycoprotein silencing with siRNA delivered by DOPE-modified PEI overcomes doxorubicin resistance in breast cancer cells. Nanomedicine (Lond). 2012 Jan; 7(1):65–78. PMID: 22191778. Pubmed Central PMCID: 3422569.

35. Moussa M, Goldberg SN, Kumar G, Sawant RR, Levchenko T, Torchilin V, et al. Radiofrequency ablation combination therapies: Does smaller adjuvant nanoparticle size translate to better outcome when combined with RF ablation? PLoS One. 2014; 9(8):e102727. doi: 10.1371/journal.pone.0102727. eCollection Epub Aug 18. PMID: 25133740

36. Sawant RR, Sriraman SK, Navarro G, Biswas S, Dalvi RA, Torchilin VP. Polyethyleneimine-lipid conjugate-based pH-sensitive micellar carrier for gene delivery. Biomaterials. 2012 May; 33(15):3942–51. PMID: 22365809. Pubmed Central PMCID: 3527089. doi: 10.1016/j.biomaterials.2011.11.088

37. Abarbanell AM, Wang Y, Herrmann JL, Weil BR, Poynter JA, Manukyan MC, et al. Toll-like receptor 2 mediates mesenchymal stem cell-associated myocardial recovery and VEGF production following acute ischemia-reperfusion injury. American journal of physiology Heart and circulatory physiology. 2010 May; 298(5):H1529–36. PMID: 20173040. Pubmed Central PMCID: 2867442. doi: 10.1152/ajpheart.01087.2009

38. Ishii H, Oota I, Takuma T, Inomata K. Developmental expression of vascular endothelial growth factor in the masseter muscle of rats. Archives of oral biology. 2001 Jan; 46(1):77–82. PMID: 11163598.

39. Eros de Bethlenfalva-Hora C, Mertens JC, Piguet AC, Kettenbach J, Schmitt J, Terracciano L, et al. Radiofrequency ablation suppresses distant tumour growth in a novel rat model of multifocal hepatocellular carcinoma. Clinical science. 2014 Feb; 126(3):243–52. PMID: 23822114. doi: 10.1042/CS20130089

40. Taylor MA, Rothwax J, Linehan WM, Wood BJ, Metwalli AR. Accelerated growth rate of multifocal renal tumors after initial radiofrequency ablation. Society of Urologic Oncology 2014; Available: http://suonet.org/pdf/ProgramBooks/2014-SUO-Program-Book.pdf:101.

41. Ahmed M, Solbiati L, Brace CL, Breen DJ, Callstrom MR, Charboneau JW, et al. Image-guided Tumor Ablation: Standardization of Terminology and Reporting Criteria-A 10-Year Update. Radiology. 2014 Jun 13:132958. PMID: 24927329.

42. de Baere T, Deschamps F, Tselikas L, Ducreux M, Planchard D, Pearson E, et al. GEP-NETS UPDATE: Interventional radiology: role in the treatment of liver metastases from GEP-NETs. European journal of endocrinology / European Federation of Endocrine Societies. 2015 Apr; 172(4):R151–R66. PMID: 25385817. doi: 10.1530/EJE-14-0630

43. Ramanathan R, Sharma A, Lee DD, Behnke M, Bornstein K, Stravitz RT, et al. Multimodality therapy and liver transplantation for hepatocellular carcinoma: a 14-year prospective analysis of outcomes. Transplantation. 2014 Jul 15; 98(1):100–6. PMID: 24503764. Pubmed Central PMCID: 4088318. doi: 10.1097/01.TP.0000441090.39840.b0

44. Hohenberger P, Kasper B, Ahrar K. Surgical management and minimally invasive approaches for the treatment of metastatic sarcoma. American Society of Clinical Oncology educational book / ASCO American Society of Clinical Oncology Meeting. 2013:457–64. PMID: 23714570. doi: 10.1200/EdBook_AM.2013.33.457

45. Gohel MS, Davies AH. Radiofrequency ablation for uncomplicated varicose veins. Phlebology / Venous Forum of the Royal Society of Medicine. 2009; 24 Suppl 1:42–9. PMID: 19307440. doi: 10.1258/phleb.2009.09s005

46. Davila ML, Hofstetter WL. Endoscopic management of Barrett's esophagus with high-grade dysplasia and early-stage esophageal adenocarcinoma. Thoracic surgery clinics. 2013 Nov; 23(4):479–89. PMID: 24199698. doi: 10.1016/j.thorsurg.2013.07.010

47. Dewire J, Calkins H. State-of-the-art and emerging technologies for atrial fibrillation ablation. Nature reviews Cardiology. 2010 Mar; 7(3):129–38. PMID: 20179720. doi: 10.1038/nrcardio.2009.232

48. Polimeni A, Curcio A, Indolfi C. Renal sympathetic denervation for treating resistant hypertension. Circulation journal: official journal of the Japanese Circulation Society. 2013; 77(4):857–63. PMID: 23514712.

49. Lim HS, Schultz C, Dang J, Alasady M, Lau DH, Brooks AG, et al. Time course of inflammation, myocardial injury, and prothrombotic response after radiofrequency catheter ablation for atrial fibrillation. Circulation Arrhythmia and electrophysiology. 2014 Feb 1; 7(1):83–9. PMID: 24446024. doi: 10.1161/CIRCEP.113.000876

50. Wu N, Xu B, Xiang Y, Wu L, Zhang Y, Ma X, et al. Association of inflammatory factors with occurrence and recurrence of atrial fibrillation: a meta-analysis. International journal of cardiology. 2013 Oct 25; 169(1):62–72. PMID: 24095158. doi: 10.1016/j.ijcard.2013.08.078

51. Deftereos S, Giannopoulos G, Kossyvakis C, Efremidis M, Panagopoulou V, Kaoukis A, et al. Colchicine for prevention of early atrial fibrillation recurrence after pulmonary vein isolation: a randomized controlled study. Journal of the American College of Cardiology. 2012 Oct 30; 60(18):1790–6. PMID: 23040570. doi: 10.1016/j.jacc.2012.07.031

52. Filgueiras-Rama D, Montoro N, Gomez-Gallanti A, Garofalo D, Peinado R. Colchicine after pulmonary vein isolation: is inflammation the new anti-arrhythmic target. Journal of the American College of Cardiology. 2013 Apr 2; 61(13):1464–5. PMID: 23433557. doi: 10.1016/j.jacc.2012.12.042

53. Guo P, Coban O, Snead NM, Trebley J, Hoeprich S, Guo S, et al. Engineering RNA for targeted siRNA delivery and medical application. Advanced drug delivery reviews. 2010 Apr 30; 62(6):650–66. PMID: 20230868. Pubmed Central PMCID: 2906696. doi: 10.1016/j.addr.2010.03.008

54. Wang J, Lu Z, Wientjes MG, Au JL. Delivery of siRNA therapeutics: barriers and carriers. The AAPS journal. 2010 Dec; 12(4):492–503. PMID: 20544328. Pubmed Central PMCID: 2977003. doi: 10.1208/s12248-010-9210-4

55. Gao Y, Liu XL, Li XR. Research progress on siRNA delivery with nonviral carriers. International journal of nanomedicine. 2011; 6:1017–25. PMID: 21720513. Pubmed Central PMCID: 3124387. doi: 10.2147/IJN.S17040

56. Hamamoto S, Okuma T, Yamamoto A, Kageyama K, Takeshita T, Sakai Y, et al. Radiofrequency ablation and immunostimulant OK-432: combination therapy enhances systemic antitumor immunity for treatment of VX2 lung tumors in rabbits. Radiology. 2013 May; 267(2):405–13. PMID: 23440322. doi: 10.1148/radiol.13120249

57. Haen SP, Pereira PL, Salih HR, Rammensee HG, Gouttefangeas C. More than just tumor destruction: immunomodulation by thermal ablation of cancer. Clinical & developmental immunology. 2011; 2011:160250. PMID: 22242035. Pubmed Central PMCID: 3254009.

58. Widenmeyer M, Shebzukhov Y, Haen SP, Schmidt D, Clasen S, Boss A, et al. Analysis of tumor antigen-specific T cells and antibodies in cancer patients treated with radiofrequency ablation. International journal of cancer Journal international du cancer. 2011 Jun 1; 128(11):2653–62. PMID: 20715115. doi: 10.1002/ijc.25601

59. Goldberg SN, Girnan GD, Lukyanov AN, Ahmed M, Monsky WL, Gazelle GS, et al. Percutaneous tumor ablation: increased necrosis with combined radio-frequency ablation and intravenous liposomal doxorubicin in a rat breast tumor model. Radiology. 2002 Mar; 222(3):797–804. PMID: 11867804.

60. Ponnappa BC. siRNA for inflammatory diseases. Current opinion in investigational drugs. 2009 May; 10(5):418–24. PMID: 19431074.